Geophysical Research Letters

RESEARCH LETTER
10.1029/2020GL091673

Key Points:

- HF-induced field-aligned plasma irregularities are simultaneously observed by GLONASS satellite and incoherent scatter radar
- The satellite signal amplitude fluctuation and TEC deviation are generally correlated
- Observed positive density deviations suggest that the density perturbations are likely caused by the thermal self-focusing process

Correspondence to:
H. Sato,
hiroatsu.sato@dlr.de

Citation:
Sato, H., Rietveld, M. T., & Jakowski, N. (2021). GLONASS observation of artificial field-aligned plasma irregularities near magnetic zenith during EISCAT HF experiment. *Geophysical Research Letters*, *48*, e2020GL091673. https://doi.org/10.1029/2020GL091673

Received 4 DEC 2020
Accepted 8 JAN 2021

GLONASS Observation of Artificial Field-Aligned Plasma Irregularities Near Magnetic Zenith During EISCAT HF Experiment

H. Sato[1], M. T. Rietveld[2,3], and N. Jakowski[1]

[1]DLR Institute for Solar-Terrestrial Physics, Neustrelitz, Germany, [2]EISCAT Scientific Association, Ramfjordbotn, Norway, [3]Department of Physics and Technology, University of Tromsø – The Arctic University of Norway, Tromsø, Norway

Abstract We report on simultaneous observation of artificial plasma density irregularities near the magnetic zenith (MZ) by incoherent scatter radar and GNSS satellite in the high latitude. During an EISCAT (European Incoherent Scatter Scientific Association) HF heating experiment, a GLONASS satellite signal intersected the disturbed ionospheric volume along the local magnetic field lines. The satellite signal amplitude and phase were simultaneously perturbed when the electron temperature increased in the F region through O-mode HF waves. The field-aligned irregularities (FAIs) and associated density perturbations are most significantly found in the MZ direction. The growth of FAI reached the saturation level in 30 s while large-scale electron density perturbation on the order of 0.1 TECU developed in a few minutes. The observed density perturbations agree well with recent numerical studies of FAI generation due to the thermal self-focusing process.

Plain Language Summary Powerful high-frequency radio waves are used to study electron heating process in the high latitude ionosphere. We observed the development of plasma density structures by analyzing small changes of amplitude and phase of ground-based satellite signals and incoherent scatter radar measurements. It is concluded that the electron heating causes irregular electron density structures along local magnetic field lines. This experiment shows that coordinated ground-based satellite and incoherent scatter radar measurements essentially help to better understand the physics of ionospheric plasma dynamics and radio wave propagation.

1. Introduction

Ionospheric modification by powerful HF radio waves has been found to be most effective when the transmitter beam is directed parallel to the Earth's magnetic field lines. These so-called magnetic zenith (MZ) effects have been found in aspect angle dependence of plasma temperature enhancements and the excitation of airglow production (Gustavsson et al., 2001; Kosch et al., 2014; Pedersen et al., 2003; M. T. Rietveld et al., 2003). The MZ effect is governed by the nonlinear self-focusing of the radio wave through the interaction with the excited striations that are strongly elongated irregularities along the field lines (A. V. Gurevich et al., 2001). The focused radio wave propagates along the magnetic field line and will cause a higher electron temperature enhancement than outside its vicinity. Plasma irregularity due to self-focusing instability has a sub-kilometer transverse scale size (Gondarenko et al., 2005). The density perturbation develops inside the field-aligned structures with a strong enhancement of the local electron temperature and density depletion at the reflection region during high-latitude HF heating (Gondarenko et al., 2006).

In situ measurement showed that the density depletion near the reflection height associated with small-scale FAI is structured in a scale of hundreds meters appearing in large groups with a radius of a few kilometers in the disturbed region (Kelley et al., 1995). The developed thermal pressure gradient can push the electrons along the magnetic field line (Liu et al., 2018; Zhou et al., 2016). Increased electron temperature or accelerated electrons can lead to an electron density enhancement at the upper/lower region along the field line. In such cases, the thermal self-focusing instability induces the large-scale field-aligned irregularities (FAIs) with a transverse scale of ~10 km.

As ionospheric disturbances due to HF heating are strongest in the MZ direction, the forming of FAI and associated electron density changes are expected to have aspect angle dependence. However, experimental evidence of such structures has not yet been reported. Probing such phenomena requires a transverse scanning of the density irregularity level near the MZ direction in the HF impact region.

Artificial bottomside layers in ionograms and positive perturbations in total electron content suggest that the bullseye optical patterns are associated with localized enhancements in plasma density below the main Artificial bottomside layers in ionograms and positive perturbations in total electron content suggest that the bullseye optical patterns are associated with localized enhancements in plasma density below the main

Using GPS L1 and L2 differential phases, Milikh et al. (2008) were the first to observe the perturbation in total electron content (TEC) in the HF heating impact region due to small-scale density irregularity induced by HAARP heating experiments. Other TEC responses to HF heating have been reported at different pump frequency resonance conditions at HAARP (Kendall et al., 2010; Najmi et al., 2014; Pedersen et al., 2009) and also at SURA experiments (e.g., Grach et al., 2018; Kunitsyn et al., 2012). A comparison of heater-induced TEC changes between GLONASS and EISCAT was reported by Tereshchenko et al. (2020). Observed HF-induced TEC enhancements should be associated with an electron temperature enhancement, but no density profile data from incoherent scatter radar data were available at HAARP and SURA. Furthermore, the diffraction of electro-magnetic signals due to ionospheric density irregularity, which results in the fluctuation and fading of the satellite signal (e.g., Kintner et al., 2007), may occur in small scales in the presence of FAIs. Such amplitude fluctuations were reported for early heating experiments with VHF beacon signals (e.g., Basu et al., 1987; Tereshchenko et al., 1998). In order to observe such effects in GNSS frequencies, coordinated experiments and precise GNSS measurements are required.

In this article, we report on simultaneous observation of HF-induced field-aligned electron temperature enhancement and density irregularities in the high latitude ionosphere through incoherent scatter radar and precise GLONASS measurements in MZ direction. The experiment was conducted by the European Incoherent Scatter (EISCAT) HF facility, UHF radar and a co-located GNSS receiver at Tromsø, Norway (69.58°N, 19.21°E).

2. Experimental Setup and Observation

On October 18, 2013, the EISCAT high-power HF facility (M. T. Rietveld et al., 2016) was operated from 12:01 to 14:00 UT for O and X mode polarization pump waves. The heating cycles were programmed for 5 min on and 2.5–3 min off intervals from 12:01 and 13:55 UT, except for 1 min off at 12:30 UT. The HF beams were directed along the magnetic zenith angle (78° elevation in the south direction). During the HF pump waves experiment, the co-located EISCAT UHF radar system at 930 MHz (Rishbeth & van Eyken, 1993) was pointed toward the field-aligned direction (77.5° elevation and 186.2° azimuth angle at 200 km altitude as of 2011) to probe the altitude variation of the electron density and temperature. The EISCAT UHF radar was analyzed using Grand Unified Incoherent Scatter Design and Analysis Package (GUISDAP) software with a time resolution of 30 s (Lehtinen & Huuskonen, 1996).

This study focuses on the HF heating from around 12:25 to 12:50 UT where the GLONASS 19 (Cosmos 2433) satellite signal passed through the heating impact region. The heating cycles are as follows: 12:25-12:30 UT (7.953 MHz, X-mode), 12:31-12:36 UT (6.20 MHz, O-mode), 12:38:30-12:43:30 UT (6.20 MHz, O-mode) and 12:46-12:51 UT (6.20 MHz, X-mode). The effective radiated power was 399.4 MW at 12:39 UT. The reflection heights for this experiment, as determined from the heights of the HF-enhanced ion line, are approximately 221 km (7.953 MHz, X-mode) and 205 km (6.20 MHz, O-mode).

Figure 1 illustrates the geometry of the GLONASS satellite track and the HF-heated volume. The Ionospheric Piercing Point (IPP) at 200 km penetrated the oval-shaped 3 dB HF contour from 12:27 UT to 12:47 UT. The GLONASS data is recorded by a 20 Hz Topcon Legacy receiver co-located at the EISCAT facilities. The GNSS receiver is able to record GLONASS L1P and L2P carrier frequencies. At 12:36 UT, the satellite elevation and azimuth angles are 78.41 and 184.5°, respectively.

Figures 2a and 2b show the electron density Ne and electron temperature T_e values along the field line as a function of altitude and time derived from the EISCAT UHF measurements. Strong temperature

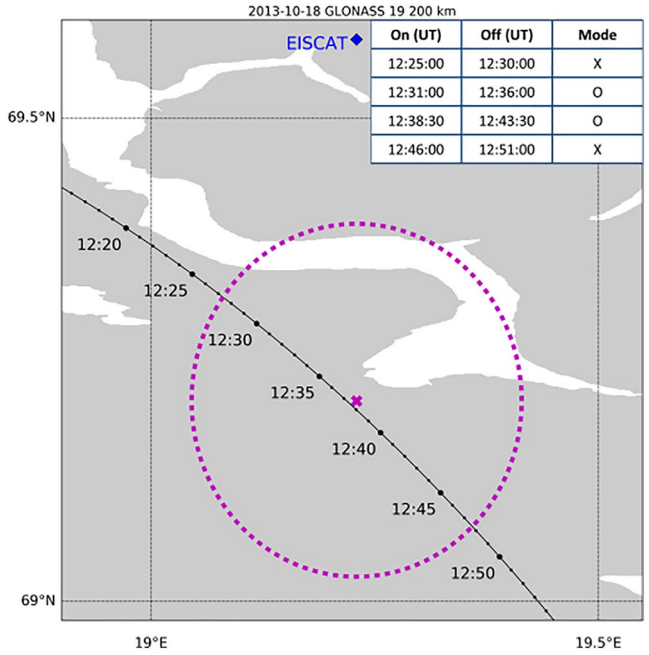

Figure 1. Trajectory of GLONASS 19 during the heating experiment on October 18, 2013. The Ionospheric Piercing Points (IPP) at a 200 km altitude seen from the GNSS receiver at EISCAT are marked with black curves. The dots between the timestamps are marked every minute. The 3 dB heater contour is shown by the purple oval and the center of the heating beam is marked by "x." The heating cycle is shown in the inserted table.

enhancement in the F region was observed for the two O-mode heating cycles from 12:31 UT to 12:36 UT and from 12:38:30 UT to 12:43:00 UT. Te increases up to 3000 K from the unperturbed levels of 1500 K from approximately 180 to 270 km with peaks at around 200 km altitude. The enhancement of Te decays to the unperturbed values within 30 s when the heating waves are turned off. The white spaces in Figure 1 represent invalid data due to large residual in the radar measurements, which occurred mostly from the reflection height of the X-mode heating until 12:30 UT (before GLONASS observation of interest in this paper).

The perturbations of the GLONASS signal are analyzed for the amplitude and differential phase data. To estimate the change in the electron density along the satellite raypath, the present study analyzes the L1 signal amplitude and TEC derived from L1 and L2 phases. GLONASS carrier frequencies are determined by the orbital plane of each satellite. For the GLONASS 19 satellite, the L1 and L2 carrier frequencies are f_1 = 1,603.6875 [MHz] and f_2 = 1,247.3125 [MHz], respectively. L1 amplitude is estimated by the raw in-phase amplitude of the L1P signal since the quadrature amplitude was not available. The amplitude fluctuation is caused by the scattering of electro-magnetic wave in an irregular medium and therefore can be used to characterize the levels of density irregularities along the satellite raypath. From L1 and L2 carrier phase group delays, on the other hand, the relative slant TEC (rSTEC) including instrumental biases can be derived by:

$$rSTEC = \left(\frac{1}{K}\right) \cdot \frac{f_1^2 f_2^2}{f_1^2 - f_2^2} \cdot \left(\lambda_1 \phi_1 - \lambda_2 \phi_2\right),$$

where ϕ_1 and $\lambda_1$are the phase and wavelength of the L1 and L2 carrier phase (cycle) and $K = 40.3\ \mathrm{m^3\ s^{-2}}$. The rSTEC are measured in TECU (1 TECU = 10^{16} electrons/$\mathrm{m^2}$) and are used to estimate the perturbation of electron density along the satellite raypath.

Figures 2c and 2d show the GLONASS L1 amplitude and rSTEC along the satellite track represented by elevation angle θ and azimuth angle φ. L1 amplitude (Figure 2c) starts to fluctuate at around 12:32 UT after entering the heating impact region during the first O-mode heating. The most significant fluctuation levels are observed from between 12:35 UT ($\theta = 78.72°, \varphi = 186.9°$) and 12:36:30 UT ($\theta = 78.41°, \varphi = 184.5°$) when the satellite raypath is nearly parallel to the local magnetic field lines, indicating that the density irregularity levels are largest near the magnetic zenith direction. After the heating off at 12:36 UT, the amplitude fluctuation is found to be decreased, but it has not completely vanished to the background levels (cf. before 12:30 UT). This indicates that there are two different decay scales in the MZ direction. The density irregularities associated with larger amplitude fluctuation decay faster (~1 min) while the smaller amplitude fluctuations are caused by the irregularities which take a longer period to decay and they do not completely disappear before the next heating on. During the second O-mode heating from 12:38:30 UT, the level of amplitude fluctuation is increased again but appeared to be weakened as the satellite goes away from the HF center. The fluctuation remained after the heating off at 12:43:30 UT and disappeared for the period after 12:45 UT including the next heating period starting at 12:46 UT, where T_e increase is not observed and the satellite is likely outside the HF impact region.

In Figure 2d, rSTEC is compared with the unperturbed rSTEC model values. Since the short time variation of STEC in the unperturbed background ionosphere is expected to be proportionate to the integration length from the ground to the satellite, the unperturbed rSTEC can be modeled by means of a simple function of the satellite elevation angle: $rSTEC \sim 1 / \sin\theta$. We used STEC data outside the heating impact region (before 12:30 and after 12:45 UT) to estimate the unperturbed values. We find that the rSTEC started to deviate simultaneously with the L1 amplitude fluctuation at 12:31 UT. The largest deviation from the unperturbed value is 0.14 TECU at 12:36:03 UT ($\theta = 78.40°, \varphi = 184.4°$). After the heating off at 12:36

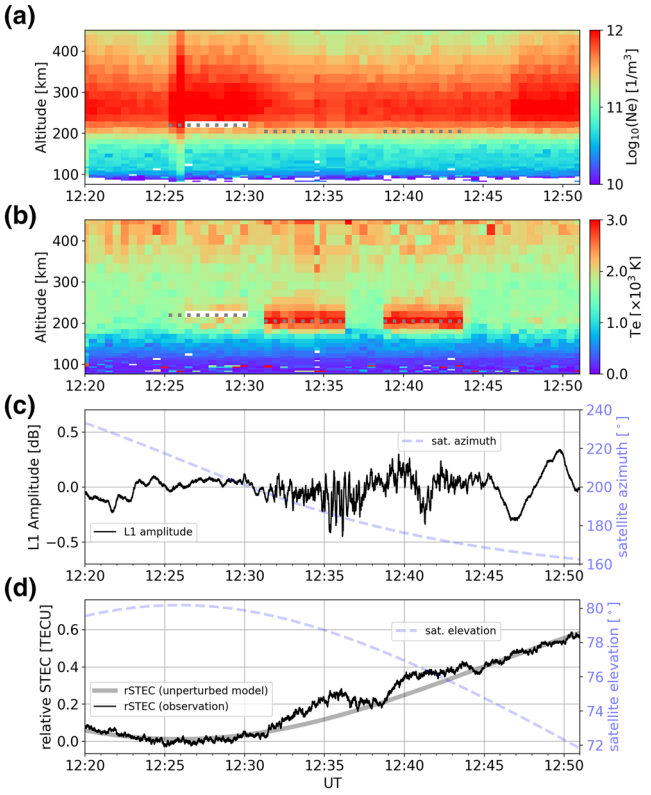

Figure 2. (a) Electron density and (b) temperature along the local magnetic field line measured by EISCAT UHF radar on October 18, 2013. The white spaces show invalid data near the reflection height. The dashed horizontal lines indicate the reflection heights. (c) GLONASS 19 L1 amplitude fluctuation. (d) Observed (black) and unperturbed (gray) relative STEC values. The satellite azimuth and elevation angles are also shown with blue dotted lines in (c) and (d), respectively. The field aligned direction is 186.2° azimuth and 77.5° elevation angle.

UT, rSTEC decreases to the unperturbed levels and increases again at the next heating on at 12:38:30 UT. During the second heating on period, the largest deviation of rSTEC is 0.12 TECU at 12:40 UT (θ = 76.95 °, φ = 176.2°), indicating that the change in rSTEC is also most significant in the MZ direction. The HF impact region for GLONASS TEC is smaller than the EISCAT HF 3db oval (see Figure 1). The more powerful HAARP facility reported scattering of the GPS signal outside its 3db oval (Milikh et al., 2008).

3. Discussion

We have shown the simultaneous response of the GLONASS carrier signal amplitude and phases to the HF heating. The density irregularities are observed to be triggered by the electron temperature increases at an altitude of 180–270 km and are most significantly enhanced in MZ direction. These satellite amplitude and TEC data show that different levels of density irregularity exist in the HF impact region.

Figures (3a and 3b) more clearly presents the enhancement of GLONASS L1 amplitude fluctuation levels over time. The time frequency representation of the L1 amplitude (Figure 3a) shows that the HF-induced FAI enhanced the amplitude fluctuation frequency f_{FAI} up to 2 Hz from the background values (f_{FAI} < 1 Hz) between 12:31 UT and 12:45 UT (79°≤ θ ≤ 74°) with the peaks of enhancement in the MZ direction. When the elevation angle is nearly parallel to the magnetic field line, we find higher frequency amplitude fluctuation (f_{FAI} > 9 Hz) is also enhanced. These higher frequency components, indicated by the white arrow in the figure, are most enhanced between 12:35 and 12:36 UT and somehow weakly enhanced between 12:39 and 12:42 UT, and are vanished during the heating off period in MZ direction. The irregularity size causing L1 amplitude fluctuation can be characterized by Fresnel dimension $(2\lambda d)^{1/2}$, where λ is L1 wavelength, and d is the distance of the irregularity from the receiver. For the irregularity height at a 220 km height, the Fresnel dimension is 290 m, and the transverse distance of amplitude fluctuation region (12:31–12:45 UT) spans 32 km around the HF beam center.

The strength of GNSS amplitude scintillations is typically quantified by the so-called S4 index, which is defined by the normalized standard deviation of signal amplitude fluctuations. We calculate this index per second from the GLONASS amplitude data in order to characterize the enhancement and decay scale of the FAI. In Figures 3b and S4 clearly increases from the background level (~0.001) by a factor of 6 when the satellite IPP enters the HF impact region. S4 levels are up by a factor of 12 near the magnetic zenith, indicating stronger scattering due to smaller scale FAI. After the heating off at 12:36 UT, S4 decreased gradually to the background level before the next heating on at 12:38:30 UT. This shows that the time scale of the irregularity decay is in the order of a few minutes. Note that even in the decay phase, the S4 value hits one of the highest levels at 12:37:11 UT in MZ direction (θ = 78.00°, φ = 181.8°). Although this enhancement of amplitude fluctuation could be interpreted as the result of remaining irregularities of HF origin, the influence of propagation geometry cannot be excluded as natural density irregularities at different altitudes can cause signal modulation. From the heating on at 12:38:30 UT, S4 again reaches a factor of 6 from the background value at 12:38:10 UT, indicating that the development of the observed irregularity is on a scale of several seconds.

The theory and numerical study of HF-induced striation predicts the bunching of striation in spatial scale of a few hundreds of meters to a few kilometer (Gondarenko et al., 2005; A. Gurevich et al., 1998). In fact, S4 data shows that the FAIs are structured rather than homogeneously generated. During 12:32–12:33 UT, for example, S4 is above the background level over the transverse scale of 2.1 km. Such structure can be found throughout the observation period. The numerically predicted time scale of bunching development is in the

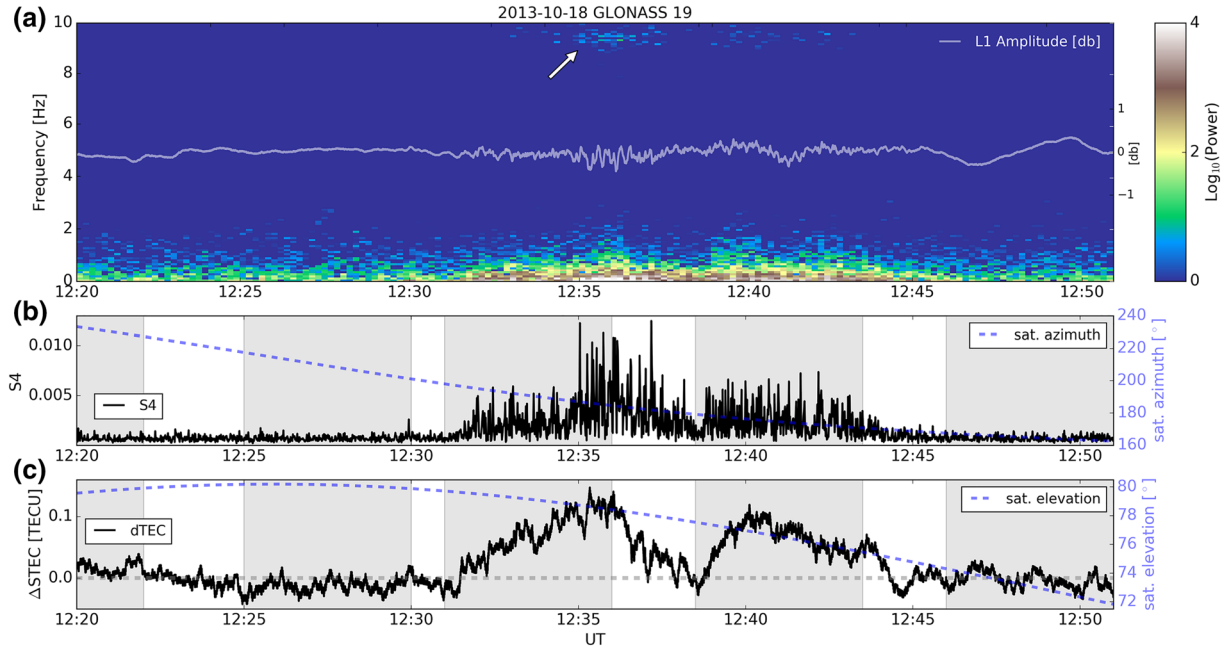

Figure 3. (a) Spectral density of GLONASS L1 amplitude fluctuation. The amplitude data is also shown in the white curve. (b) S4 index per second of GLONASS L1 amplitude (black curve) and satellite azimuth angle (blue dotted curve). (c) STEC deviation from unperturbed values (black) and satellite elevation (blue dotted curve). The shaded gray areas show the heating on periods.

scale of 100 ms. Current satellite measurement resolution is not able to observe precisely the development of bunching within this time scale. The production of larger-scale striations is thought to be the result from merging of smaller striations due to the ponderomotive force caused by the interaction of small-scale striation and the HF wave (Istomin & Leyser, 2010).

Figure 3c shows the deviation of rSTEC from the unperturbed values:$\Delta STEC = rSTEC_{obs} - rSTEC_{\mathrm{model}}$. We find that the $\Delta STEC$ as a response to the EISCAT heating experiment (max. 0.14 TECU) is at a similar magnitude as that observed at HARRP (Najmi et al., 2014). The observed enhancements of STEC are generally well correlated with the amplitude fluctuations. We note the different evolution time for the HF-induced small-scale irregularity and for the large-scale electron density modification during the heating on starting at 12:38:30 UT. While S4 reaches the next maximum value of 0.0057 at 12:38:50 UT, $\Delta STEC$ hits the local maximum value of 0.1 TECU at a later time of 12:40:02 UT. These results show the different evolution time scale of FAI and the associated electron density enhancement. FAI reaches the stationary conditions on a time scale of a few tens of seconds. This time scale corresponds to the saturation time due to thermal self-focusing instability (Kosch et al., 2007). Numerical simulation shows that the growth of large-scale density perturbation in the scale of 10% requires 180 s after HF on (Liu et al., 2018).

Here we discuss the electron density perturbation observed by means of EISCAT Ne. Figure 4 shows EISCAT Ne and T_e comparison during HF on and off periods averaged over two O-mode HF heating cycles between 12:31 UT and 12:43:30 UT. T_e increases at the height of the F region with the peak up to 65% (7.9% estimated error) at around 200 km altitude from the off period. The Ne profile shows both increases and decreases during the heating on periods. Although a tendency of Ne decrease can be found at an altitude between 200 and 300 km where T_e increases significantly, both an increase and decrease of Ne are observed in this altitude where the significant increase of T_e may cause a strong pressure gradient as the largest decrease of 5.2% (2.0% estimated error) is found between 280 and 300 km. Above and below the peak T_e enhancement altitude, an increase of Ne up to 10% (3.9%–4.2% estimated error) is found at an altitude below 200 and above 400 km.

Significant density enhancements have been reported in the ionogram below the main F region and positive perturbation of GPS TEC during the powerful HF heating by HAARP (Pedersen et al., 2009). Such a density enhancement can be explained by means of an acceleration of electrons through an HF beam, which leads

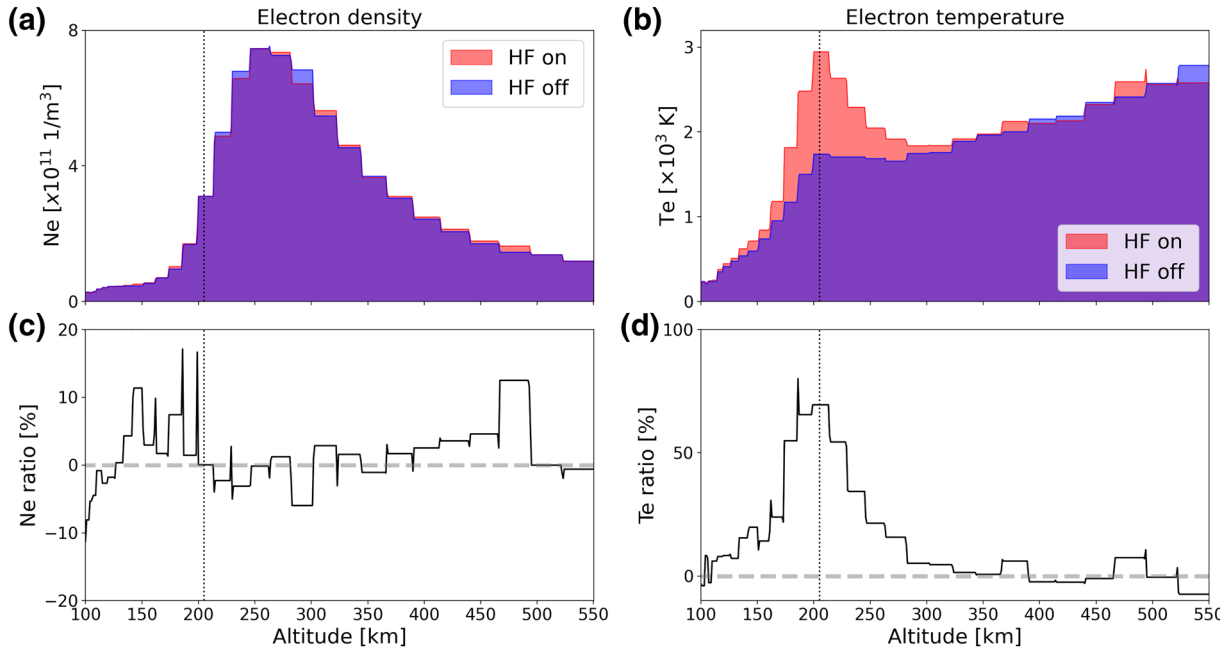

Figure 4. EISCAT T_e and Ne profiles averaged over two O-mode HF cycles. (a–b) Ne and T_e profile comparison in HF on and off periods. (c–d) Ne and T_e increase ratio during HF on compared to HF off. The dotted vertical line indicates the reflection height.

to push the density away from the reflection height at a scale of a few minutes. Localized enhancement of electron density may be explained by suppression of recombination due to increased electron temperature or by the ionization by accelerated suprathermal electrons. Numerical simulation shows the electron density depletion associated with temperature enhancement at the reflection region (Gondarenko et al., 2006), which leads to the upper and lower region through the large-scale thermal diffusion along the field line (Liu et al., 2018; Zhou et al., 2016). Indeed, in our experiment, the electron density increases both above and below the reflection height and a positive density deviation is observed by both incoherent scatter radar and GLONASS measurements.

In order to quantitatively compare EISCAT Ne with GLONASS TEC, we calculate TEC values along the EISCAT Ne profile by $STEC_{eiscat} = \int_{h1}^{h2} Ne\, dh$, where h1 and h2 are the lower and the upper limit of the height integral. With h1 = 100 km and h2 = 500 km, $STEC_{eiscat}$ along the slant range resulted in 13.02 TECU (HF on 12:31–12:36:00 UT), 12.78 TECU (HF off, 12:36:00–12:38:30 UT), 12.80 TECU (HF on 12:38:30–12:43:30 UT) and 12.71 TECU (HF off, 12:43:30–12:46:00 UT). When averaged over two heating cycles, STEC increased by $\Delta STEC_{eiscat} = 0.16$ TECU, which quantitatively agrees with the largest GLONASS $\Delta STEC$ in the MZ direction, considering GLONASS STEC contains a change of electron density contribution outside EISCAT measurement between the satellite altitude and ground.

4. Conclusion

In this article, we have presented simultaneous observation of HF-induced field aligned density irregularities near the magnetic zenith in a high-latitude F region by means of incoherent scatter radar and precise GLONASS signal measurements. We show direct evidence of the MZ effect on the generation of FAI and associated electron density perturbation due to HF-induced electron temperature enhancement. The satellite measurements show that the enhancements of TEC are generally well correlated with the amplitude fluctuations. The growth time of FAI is on the scale of 30 s and the increase of electron density is on the order of a few minutes. The electron density increases both above and below the reflection height and a positive density deviation is observed by both incoherent scatter radar and GLONASS measurements. The

enhancement level of the EISCAT electron density and GLONASS TEC during HF on periods are generally in agreement. The results suggest that the observed density irregularity is generated by the electrons pushed up and down along the magnetic field lines by HF heating. The development of the density irregularities corresponds well to the thermal self-focusing mechanism reported in previous studies.

This study shows the high rate GNSS data along with incoherent scatter radar can be used to study small scale density perturbation induced by HF heating. One of the recently debated topics in the ionospheric active experiment research is aspect angle-dependent density enhancement during X mode heating at EISCAT (Blagoveshchenskaya et al., 2011a, 2011b; M. Rietveld & Senior, 2020; Senior et al., 2013; Wang & Zhou, 2017). In fact, an apparent density increase was observed through X-mode heating in EISCAT Ne before the GLONASS passing (see 12:26 UT in Figure 2). A future study is expected to use the presented experimental setup to diagnose the density perturbation of X-mode heating.

Data Availability Statement

All data used within the publication are available from an online repository (http://doi.org/10.5281/zenodo.4305577) or on request to the email address impc-uhd@dlr.de

Acknowledgment
EISCAT is an international association supported by research organizations operating in China (CRIRP), Finland (SA), Japan (NIPR and STEL), Norway (NFR), Sweden (VR) and the United Kingdom (NERC). Open access funding enabled and organized by Projekt DEAL.

References

Basu, S. S., Basu, S. S., Stubbe, P., Kopka, H., & Waaramaa, J. (1987). Daytime scintillations induced by high-power HF waves at Tromsø, Norway. *Journal of Geophysical Research*, *92*(A10), 11149–11157. https://doi.org/10.1029/JA092iA10p11149

Blagoveshchenskaya, N. F., Borisova, T. D., Rietveld, M. T., Yeoman, T. K., Wright, D. M., Rother, M., et al. (2011b). Results of Russian experiments dealing with the impact of powerful HF radiowaves on the high-latitude ionosphere using the EISCAT facilities. *Geomagnetism and Aeronomy*, *51*(8), 1109–1120. https://doi.org/10.1134/s0016793211080160

Blagoveshchenskaya, N. F., Borisova, T. D., Yeoman, T. K., Rietveld, M. T., Ivanova, I. M., & Baddeley, L. J. (2011a). Artificial small-scale field-aligned irregularities in the high latitude F region of the ionosphere induced by an X-mode HF heater wave. *Geophysical Research Letters*, *38*(8), L08802. https://doi.org/10.1029/2011GL046724

Gondarenko, N. A., Ossakow, S. L., & Milikh, G. M. (2005). Generation and evolution of density irregularities due to self-focusing in ionospheric modifications. *Journal of Geophysical Research*, *110*(A9), 1–13. https://doi.org/10.1029/2005JA011142

Gondarenko, N. A., Ossakow, S. L., & Milikh, G. M. (2006). Nonlinear evolution of thermal self-focusing instability in ionospheric modifications at high latitudes: Aspect angle dependence. *Geophysical Research Letters*, *33*(16), L16104. https://doi.org/10.1029/2006GL025916

Grach, S. M., Nasyrov, I. A., Kogogin, D. A., Shindin, A. V., Sergeev, E. N., & Razi Mousavi, S. A. (2018). Mutual allocation of the artificial airglow patches and large-scale irregularities in the HF-pumped ionosphere. *Geophysical Research Letters*, *45*(23), 12749–12756. https://doi.org/10.1029/2018GL080571

Gurevich, A. V., Carlson, H., & Zybin, K. P. (2001). Nonlinear structuring and southward shift of a strongly heated region in ionospheric modification. *Physics Letters A*, *288*(3–4), 231–239. https://doi.org/10.1016/S0375-9601(01)00516-3

Gurevich, A., Hagfors, T., Carlson, H., Karashtin, A., & Zybin, K. (1998). Self-oscillations and bunching of striations in ionospheric modifications. *Physics Letters A*, *239*(6), 385–392. https://doi.org/10.1016/S0375-9601(98)00006-1

Gustavsson, B., Sergienlo, T., Rietveld, M. T., Honary, F., Steen, A., Brändström, U. E., et al. (2001). First tomographic estimate of volume distribution of HF-pump enhanced airglow emission. *Journal of Geophysical Research*, *106*(A12), 29105–29123. https://doi.org/10.1029/2000JA900167

Istomin, Y. N., & Leyser, T. B. (2010). Kinetics of density striations excited by powerful electromagnetic waves in the ionosphere. *Physics of Plasmas*, *17*(3), 032903. https://doi.org/10.1063/1.3356085

Kelley, M. C., Arce, T. L., Salowey, J., Sulzer, M., Armstrong, W. T., Carter, M., & Duncan, L. (1995). Density depletions at the 10-m scale induced by the Arecibo heater. *Journal of Geophysical Research*, *100*(A9), 17367–17376. https://doi.org/10.1029/95JA00063

Kendall, E., Marshall, R., Parris, R. T., Bhatt, A., Coster, A., Pedersen, T., et al. (2010). Decameter structure in heater-induced airglow at the High frequency Active Auroral Research Program facility. *Journal of Geophysical Research*, *115*(8), 1–11. https://doi.org/10.1029/2009JA015043

Kintner, P. M., Ledvina, B. M., & de Paula, E. R. (2007). GPS and ionospheric scintillations. *Space Weather*, *5*(9), S09003. https://doi.org/10.1029/2006SW000260

Kosch, M. J., Bryers, C., Rietveld, M. T., Yeoman, T. K., & Ogawa, Y. (2014). Aspect angle sensitivity of pump-induced optical emissions at EISCAT. *Earth, Planets and Space*, *66*(1), 159. https://doi.org/10.1186/s40623-014-0159-x

Kosch, M. J., Pedersen, T., Mishin, E., Starks, M., Gerken-Kendall, E., Sentman, D., et al. (2007). Temporal evolution of pump beam self-focusing at the high-frequency active auroral research program. *Journal of Geophysical Research*, *112*(8), 1–9. https://doi.org/10.1029/2007JA012264

Kunitsyn, V. E., Andreeva, E. S., Frolov, V. L., Komrakov, G. P., Nazarenko, M. O., & Padokhin, A. M. (2012). Sounding of HF heating-induced artificial ionospheric disturbances by navigational satellite radio transmissions. *Radio Science*, *47*(4), 1–13. https://doi.org/10.1029/2011RS004957

Lehtinen, M. S., & Huuskonen, A. (1996). General incoherent scatter analysis and GUISDAP. *Journal of Atmospheric and Terrestrial Physics*, *58*(1–4), 435–452. https://doi.org/10.1016/0021-9169(95)00047-X

Liu, M., Zhou, C., Wang, X., Bin Ni, B., & Zhao, Z. (2018). Numerical simulation of oblique ionospheric heating by powerful radio waves. *Annals of Geophysics*, *36*(3), 855–866. https://doi.org/10.5194/angeo-36-855-2018

Milikh, G., Gurevich, A., Zybin, K., & Secan, J. (2008). Perturbations of GPS signals by the ionospheric irregularities generated due to HF-heating at triple of electron gyrofrequency. *Geophysical Research Letters*, *35*(22), L22102. https://doi.org/10.1029/2008GL035527

Najmi, A., Milikh, G., Secan, J., Chiang, K., Psiaki, M., Bernhardt, P., et al. (2014). Generation and detection of super small striations by F region HF heating. *Journal of Geophysical Research – A: Space Physics*, *119*(7), 6000–6011. https://doi.org/10.1002/2014JA020038

Pedersen, T., Gustavsson, B., Mishin, E., MacKenzie, E., Carlson, H. C., Starks, M., & Mills, T. (2009). Optical ring formation and ionization production in high-power HF heating experiments at HAARP. *Geophysical Research Letters*, *36*(18), 2–5. https://doi.org/10.1029/2009GL040047

Pedersen, T. R., McCarrick, M., Gerken, E., Selcher, C., Sentman, D., Carlson, H. C., & Gurevich, A. (2003). Magnetic zenith enhancement of HF radio-induced airglow production at HAARP. *Geophysical Research Letters*, *30*(4), 1169. https://doi.org/10.1029/2002GL016096

Rietveld, M. T., Kosch, M. J., Blagoveshchenskaya, N. F., Kornienko, V. A., Leyser, T. B., & Yeoman, T. K. (2003). Ionospheric electron heating, optical emissions, and striations induced by powerful HF radio waves at high latitudes: Aspect angle dependence. *Journal of Geophysical Research*, *108*(A4), 1141. https://doi.org/10.1029/2002JA009543

Rietveld, M., & Senior, A. (2020), Ducting of incoherent scatter radar waves by field-aligned irregularities, *Annals of Geophysics*, *38*, 1101–1113. https://doi.org/10.5194/angeo-2020-22

Rietveld, M. T., Senior, A., Markkanen, J., & Westman, A. (2016). New capabilities of the upgraded EISCAT high-power HF facility. *Radio Science*, *51*(9), 1–14. https://doi.org/10.1002/2016RS006093

Rishbeth, H., & van Eyken, A. P. (1993). EISCAT: Early history and the first ten years of operation. *Journal of Atmospheric and Terrestrial Physics*, *55*(4–5), 525–542. https://doi.org/10.1016/0021-9169(93)90002-G

Senior, A., Rietveld, M. T., Häggström, I., & Kosch, M. J. (2013). Radio-induced incoherent scatter ion line enhancements with wide altitude extents in the high-latitude ionosphere. *Geophysical Research Letters*, *40*(9), 1669–1674. https://doi.org/10.1002/grl.50272

Tereshchenko, E. D., Cherniakov, S. M., Yurik, R. Y., Rietveld, M. T., & Häggström, I. (2020). Total electron content measurements in the ionosphere disturbed by high-power high-frequency waves by the methods of incoherent scattering of radio waves and radio sounding by glonass satellite signal. *Radiophysics and Quantum Electronics*, *62*(10), 667–676. https://doi.org/10.1007/s11141-020-10012-4

Tereshchenko, E. D., Khudukon, B. Z., Rietveld, M. T., & Brekke, A. (1998). Spatial structure of auroral day-time ionospheric electron density irregularities generated by a powerful HF-wave. *Annals of Geophysics*, *16*(7), 812–820. https://doi.org/10.1007/s00585-998-0812-4

Wang, X., & Zhou, C. (2017). Aspect dependence of Langmuir parametric instability excitation observed by EISCAT. *Geophysical Research Letters*, *44*(18), 9124–9133. https://doi.org/10.1002/2017GL074743

Zhou, C., Ni, B., Wang, X., Liu, M., Xu, X., Wang, C., et al. (2016). A numerical study of large-scale ionospheric modulation due to the thermal process by powerful wave heating. *Journal of Geophysical Research - A: Space Physics*, *121*(3), 2704–2714. https://doi.org/10.1002/2016JA022355